Two-regime kinetic study and parameter optimization of degradation of 3,4-dichloroaniline using TI–N/S catalyst under visible light

Padmini Ellappan, Lima Rose Miranda*

Carbon Research and Engineering, Department of Chemical Engineering, A.C. Tech, Anna University, Chennai 600 025, Tamil Nadu, India, Tel. +91 9962564560; email: padminisutha@gmail.com (P. Ellappan), Tel. +91 9444827462; email: limamiranda2007@gmail.com (L.R. Miranda)

ABSTRACT

This paper presents the research of the effects of operating parameters on the photocatalytic degradation of 3,4-dichloroaniline (3,4-DCA) using non-metal doped TiO_2-based photocatalysts. The nitrogen- and sulfur-doped in TiO_2 which was prepared using sol–gel method. The prepared catalyst was characterized using XRD, SEM-EDX, FTIR, XPS, DRS, and BET analysis. The characterization revealed that Ti–N showed lower particle size, higher specific surface area, and low band-gap energy as compared to Ti–S. The photocatalytic degradation of 3,4-DCA using Ti–N showed better activity as compared to Ti–S and undoped TiO_2. The findings revealed that various parameters, such as the initial pH of the solution to be degraded, catalyst loading, concentration of solution, and light intensity, exert their individual influence on the photocatalytic degradation of 3,4-DCA. The kinetics of degradation of 3,4-DCA followed two-regime LH model and rate constants were determined. The reaction constant and Langmuir adsorption constants were determined and half-life time which was determined was found to be closer to those determined using two-regime fit.

Keywords: 3,4-dichloroaniline; Photocatalysis; Non-metal doping; Nitrogen; Optimization

1. Introduction

3,4-Dichloroaniline (3,4-DCA) is an aromatic amine and is widely used as synthesis chemical and chemical intermediates in production of several herbicides and azo dyes. The major part of the 3,4-DCA was processed to 3,4-dichlorophenylisocyanate by reaction with phosgene. It was also formed as an intermediate product during the degradation of cosmetic chemical, trichlorocarbanilide. 3,4-DCA is also formed in industrial wastewater treatment plants by microbial transformation of 3,4-dichloro-nitrobenzene (BUA, 1990).

This compound can be released into the wastewater during its production and processing thus leading to an emission of 3,4-DCA. 3,4-DCA is also a metabolite of the herbicide propanil. Formation from propanil occurs by hydrolysis, by microorganisms in soil and in rice field water, and by enzymes in plants [1].

Researchers have developed new and inexpensive methods for the treatment of 3,4 DCA which could be broadly classified as physical, chemical and biological methods. Processes such as reduction oxidation, complexometric method, and ion exchange and neutralization techniques have been categorized as chemical methods. Biological methods are those involving the usage of microorganisms in the presence or absence of

*Corresponding author.

oxygen, that is, aerobic and anaerobic process. Physical process methods such as adsorption and filtration have also been used to degrade 3,4-DCA.

However, a potential harmless and powerful method for transforming pollutants with high degree of process flexibility is the advanced oxidation process (AOP). AOPs offer high ability in degradation of any concentration of the pollutants, which is the main drawback of physical and biological treatment methods. Several features, such as ambient operating conditions, complete destruction of parents and their intermediate compounds, and relatively low operating cost, have confirmed photocatalysis applicability to water treatment. Previous study on degradation of 3,4-DCA using cerium- and vanadium-doped semiconductor catalyst showed complete degradation, and also, there was no formation of harmful intermediates [2].

In AOP, the reactor in which the degradation was carried out classified as slurry, immobilized reactors based on the nature of addition of catalyst and photoelectrocatalytic reactors where, in addition to photon generation, electrolytic process also combined with AOP to degrade the compounds. In slurry reactors, the catalysts are suspended and are uniformly distributed throughout the reactor. With the slurry system, an additional process step would need to be entailed for post-separation of the catalysts. To overcome this difficulty, the catalysts are immobilized on different materials such as activated carbon [3], mesoporous clays [4], fibers [5], and into the membrane itself [6]. There are also various hybrid systems, which includes the usage of electrolytic process along with the photocatalytic process [7].

The most commonly used catalyst is TiO$_2$, and the popularity of TiO$_2$ as a photocatalyst is based on its environmentally friendly nature (i.e. non-toxicity), low cost, chemical stability, high natural abundance, and versatile potential applications [8,9]. In order to utilize TiO$_2$ to its full potential, it is necessary to decrease the band-gap size facilitating visible light absorption. Non-metal doping has shown great promise in achieving visible light-activated photocatalysis, with nitrogen being the most effective dopant. Doping of TiO$_2$ with transition metals such as Cr, Co, V, and Fe has extended the spectral response of TiO$_2$ well into the visible region also improving photocatalytic activity [10–12]. Deposition of noble metals such as Ag, Au, Pt, and Pd on the surface of TiO$_2$ enhances the photocatalytic efficiency under visible light by acting as an electron trap, promoting interfacial charge transfer, and therefore delaying recombination of the electron–hole pair [13–15]. Many efforts have been made in the synthesis of different coupled semiconductors such as ZnO/TiO$_2$, CdS/TiO$_2$ [16], and Bi$_2$S$_3$/TiO$_2$ [17]. The

disadvantages of the individual components were also compensated and induced a synergistic effect such as an efficient charge separation and improvement of photostability [18].

This research paper aims at degrading 3,4-DCA using non-metal doped titania. The non-metals used for doping chosen for this research is nitrogen and sulfur. This paper also explains in detail the influence of the operational parameters and the kinetics of degradation.

2. Materials and methods

2.1. Chemicals and materials

The chemicals used for the preparation of catalyst were titanium isopropoxide (Sigma–Aldrich), ethanol (Central drug house, Mumbai), glacial acetic acid (Sigma–Aldrich), isopropanol (Central drug house, Mumbai), nitric acid (Central drug house, Mumbai), ammonia (Central drug house, Mumbai), and sodium sulfate (SRL, Mumbai).

The model pollutant used was 3,4-dichloroaniline (Sigma–Aldrich). The pH of the solution was changed by addition of hydrochloric acid (Central drug house, Mumbai) or sodium hydroxide (Central drug house, Mumbai). The water used for preparing all the solutions was distilled water.

2.2. Preparation of non-metal doped catalyst

The N-doped TiO$_2$ was synthesized by the following technique: an aqueous titanium isopropoxide (TTIP) was prepared by 20 wt % of TTIP and 80 wt % of ethanol, and then, the ready solution was hydrolyzed in a magnetic stirring apparatus by the addition of 30% NH$_3$ aqueous solution until the pH of the mixture reached 7. The hydrolysis product, which is in the form of white suspended semi-solid, was rinsed with distilled water. Finally, dried at 120°C for 24 h and calcined at 500°C for 4 h.

For the synthesis of the S-doped TiO$_2$ powder, sol of TiO$_2$ was mixed with thiourea (CS (NH$_2$)$_2$) and hydrochloric acid (HCl) at a molar ratio of 1:3 in ethanol. The solution was stirred at 80°C for 2 h and concentrated under reduced pressure. After evaporation of ethanol, white slurry was obtained. The slurry was kept for 24 h at 100°C in oven, and a yellow powder was obtained. This powder was calcined in the furnace at 500°C for 4 h.

2.3. Catalyst Characterization

The crystalline phase was obtained by a Philips Pw 1830 X-ray diffractometer (XRD) operated at 40 kV

and 35 mA and a Philips X' Pert X-ray diffractometer operated at 40 kV and 30 mA, both of which used Cu Kα radiation source at λ of 1.54 Å. Scherrer's equation was used to calculate the crystallite as shown in Eq. (1) [19].

$$D = \frac{k\lambda}{\beta \cos \theta} \tag{1}$$

where D is the crystallite size (nm)

k is the constant whose value is approximately 0.9

λ is the wavelength of the X-ray radiation source (0.154 nm for Cu Kα)

β is the full width at half maximum intensity (radians)

θ_B is the Bragg angle at the position of the peak maximum

The anatase content was also calculated applying Spurr–Myers equation as shown in Eq. (2) [20].

$$w_A = \frac{1}{1 + 1.26\, I_R/I_A} \tag{2}$$

where w_A is the weight fraction of anatase in the mixture

I_R is the intensity of the diffraction peak of rutile

I_A is the intensity of the diffraction peak of anatase

The specific surface area of the catalysts was determined by nitrogen adsorption at 77 K by BET Quanta chrome instrument. All the samples received a preliminary heat treatment at 100–120°C under 10^{-2} Torr vacuum for 4 h to eliminate the trace amount of water present in the samples. The specific surface area was calculated using the BET method.

The particle size was also calculated using surface area calculated from BET isotherms determined using BET Quanta chrome instrument as given in Eq. (3).

$$\text{Particle diameter } d = \frac{6{,}000}{S_{\text{BET}} \times \rho} \tag{3}$$

where S_{BET} is the surface area (m^2 g^{-1}) and ρ is the density of the catalyst which is approximately 4.2 gcm^{-3} for titania-based particles.

SEM–EDX analysis was performed to evaluate the morphology of the amorphous starting material and the obtained well-crystallized catalysts on a *Hitachi S-4700 Type II* cold field emission scanning electron microscope equipped with a *Röntec QX2-EDS* spectrometer.

The DRS spectra of all the samples were recorded to determine the sample's UV–vis light absorption capacity, on a *Jasco-V650* diode array, computer

controlled (with *Spectra Manager software*) spectrophotometer equipped with an *ILV-724* integration sphere. The band-gap energy was calculated using the Kubelka–Munk units (f(R)) obtained by the conversion of reflectance value determined by UV-DRS analysis. The graph was plotted between (f(R) h × v)^2 vs. h × v. Band-gap energy can be calculated from the *Eg* value which is obtained by extrapolating the linear portion to the photon energy axis in the plot.

XPS technique provides a compositional estimate of only the outermost layers, with a penetration depth of *ca.* 5–15 nm. X-ray photoelectron spectroscopy (XPS) was used to analyze the atomic surface concentration on each catalyst. The spectra were recorded on a Perkin-Elmer model 5300 X-ray photoelectron spectrometer using Mg Kα-1253.6 eV as a radiation source at 300 W.

FTIR spectroscopic measurements were obtained using a Perkin-Elmer System 2000 spectrometer. The resolution was 4 cm^{-1}. The catalyst was pressed in KBr pellets, and the IR spectra were recorded between 4,000 and 400 cm^{-1}. The FTIR spectra analyze the possible functional groups on the catalyst particles.

Zeta potential of the catalyst was measured using zeta-meter 4.

2.4. Photocatalytic reactor setup

The photocatalytic reactor used in this study is an annular reactor with a lamp placed inside the immersion well as illustrated in Fig. 1. The lamp is cooled with cooling water circulated in the jacket. The reactor used was 30 cm in length with the annular volume capacity of 1,000 mL. The solution along with the catalyst is taken in the annular region and is continuously
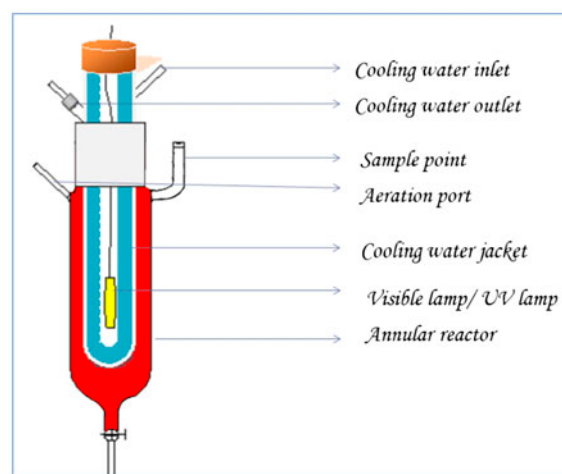

Fig. 1. Photocatalytic reactor setup.

stirred for homogeneity. The reactor has a sample port from which samples are withdrawn at noted time intervals. The sample is centrifuged before analysis of concentration.

Visible lamps with wavelength of 365 to 700 nm and 150, 300, 500 W intensity were used for performing degradation under visible region. The visible lamps are directly connected to the A/C supply.

2.5. Degradation experiment

The parameters studied in this research are given in Table 1. The aqueous solution is taken in the annular region of the reactor. The solution was mixed well, and then, the required lamp placed in the immersion well. For photolysis experiments, experiments were performed in the absence of catalyst and irradiation was done for 7 h.

In the case of the visible light irradiation, the experiment was conducted after allowing the solution to equilibrate for one hour in dark, that is, dark adsorption in the presence of required amount of catalyst. After an hour, the lamp was switched on and stirring was kept constant. Samples were removed at known intervals of time, and the samples were centrifuged for 10 min to remove the suspended catalyst. The clear supernatant solution was then analyzed for the concentration, while the catalyst was recycled into the reactor. The percentage degradation was calculated using the Eq. (4)

$$\% \, degradation = \frac{C_0 - C}{C_0} \times 100 \qquad (4)$$

where C_0 = initial concentration of the solution, $mg \, L^{-1}$
   C = Concentration of the solution at time t, $mg \, L^{-1}$

2.6. Spectrophotometric determination of DCA

The concentration of the aqueous solution at various times was determined using a Hitachi (U 2000)

Table 1
Parameters and range studied in photocatalytic degradation

Parameters	Range
Compound studied	3,4-Dichloroaniline (DCA)
Concentration, $mg \, L^{-1}$	5, 10, 15, 20, 25, 30
Visible lamp intensity, W	150, 300, 500
Catalyst dosage, gL^{-1}	0.01–0.15
pH	2, 4, 6, 8, 10, 12
Temperature ℃	32

UV–vis spectrophotometer. To every 0.4 mL of the sample 2 mL of 0.1 N, HCl was added and mixed well. To this solution, 1.4% sodium nitrite was added. To destroy excess nitrite, ammonium sulfamate was added and allowed to stand for 10 min. After 10 min, a purple complex which was formed by the addition of β-napthol was analyzed at 540 nm wavelength.

2.7. TOC analysis

The photomineralization of the compounds was measured using total organic carbon analyzer (Shimadzu TOC 5000 A).

3. Results and discussion

3.1. Catalyst characterization

The crystallite size of the catalyst Ti–N and Ti–S and the phase composition were analyzed and compared by performing XRD analysis as seen in Figs. 2 and 3. The peaks at $2\theta = 27°$, 36°, and 54.3° indicate the presence of the TiO_2 in the rutile phase, while peaks at $2\theta = 25.5°$, 37.2°, 48°, and 62.6° indicate the presence of the anatase phase. Both the samples contained rutile and anatase phases, the difference was in the relative amounts as shown by the intensity of the peaks. N-doped showed that it contains almost no rutile phase while that for S-doped Ti and indicated that there was more of rutile phase formation with the standard peak at 27.3°. The average crystallite size calculated using Scherer's equation for Ti–N and Ti–S was 6.23 nm and 11.24 nm, respectively.

The specific surface area, pore volume, and pore radius for the Ti–N and Ti–S were determined using BET method and N_2 adsorption–desorption isotherms
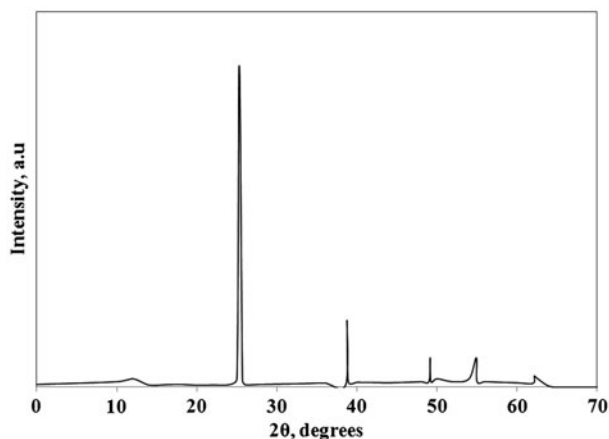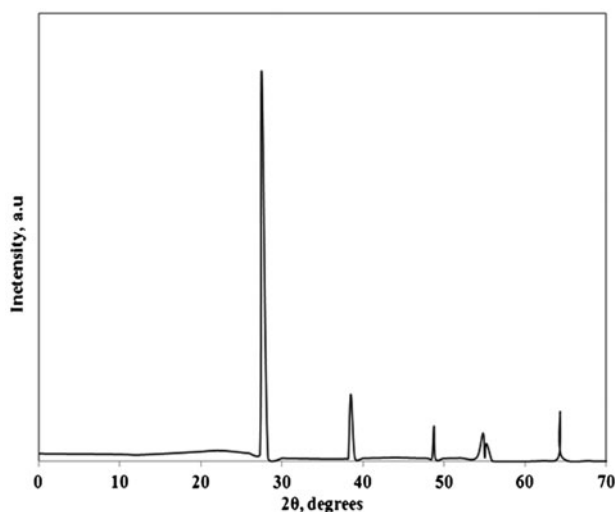

Fig. 2. XRD analysis of Ti–N.

Fig. 3. XRD analysis of Ti–S.

and are as shown in Table 2. The specific surface area for Ti–N was larger, while Ti–S was lesser. Particle size calculated based on the specific surface area was in concurrence to the XRD analysis. The pore volume and pore radius were the highest for Ti–N as compared to the other catalyst.

The higher the specific surface area for adsorption of contaminants, the higher the photocatalytic efficiency since only the molecules that are in direct contact with the catalyst surface undergo degradation. Also, the smaller the particle size the shorter the distance the charge carrier travels to the surface where the reaction occurs. This could increase the photoactivity of the catalyst along with the reduction in degradation time.

The surface morphology was studied using SEM analysis as shown in Fig. 4. For Ti–N catalyst, the particles are almost spherical and uniformly distributed. Ti–S shows agglomeration with varied sizes of particles. The elemental composition of the various catalyst samples was estimated by EDX and compared in

Table 2 and illustrated in Fig. 5. The principal components of the materials are characterized, and the percentage of each atomic element was calculated. Oxygen element was present in both the catalyst confirming that the oxides were formed during the preparation of catalyst. Spectra of both the catalyst showed that the catalyst was of high purity and they didn't show peaks of any other elements except the dopant.

The UV–vis spectra of Ti–N and Ti–S show a continuous, tailing absorption spectrum in the visible region as seen in Fig. 6. The band-gap energy of Ti–N was determined as 2.23 eV and that for Ti–S was 3.34 eV, by the plot of the modified Kubelka–Munk function vs. photon energy.

The doping of nitrogen and boron into the TiO_2 lattice and its state was substantiated and measured by XPS. Fig. 7(a) illustrates the Ti 2p, O1s and N1s, spectra of Ti–N catalyst. In N1s XPS spectra, two signals at BE = 394.17 eV and 401.12 eV could be observed. The peak at 394.17 eV belongs to βN state, and attributing to the presence of Ti–N bond whereby the N atoms replace the oxygen atoms in TiO_2 lattice. The second peak at 401.12 eV may be due to molecularly adsorbed nitrogen-containing compound on the surface [21]. The presence of titania ion in an octahedral environment is indicated by major peak which is centered at 462.83 eV in the Ti_{2p} spectra. There is a single major peak that is observed at 534.45 eV in case of O1s, which corresponds to Ti–O bond.

Fig. 7(b) confirms the existence of Ti, O, and S elements on the surface of the Ti–S is confirmed. Ti $(2p_{3/2})$ core level at binding energy of 458.1 eV asserts the existence of titanium in the form of Ti^{4+} state solely. O (1s) peak which can be deconvoluted into three components. The peak located at the binding energy of 529.4 eV and is assigned to the crystal lattice oxygen (Ti–O). The peaks located at the binding energies of 530.45 and 531.4 eV, respectively and represent the oxygen in the S–O–Ti and S–O–S groups. The S 2p peaks can be resolved into two components demonstrating that there are two kinds of S-binding states in the layers.

Table 2
Physico-chemical properties of Ti–N and Ti–S

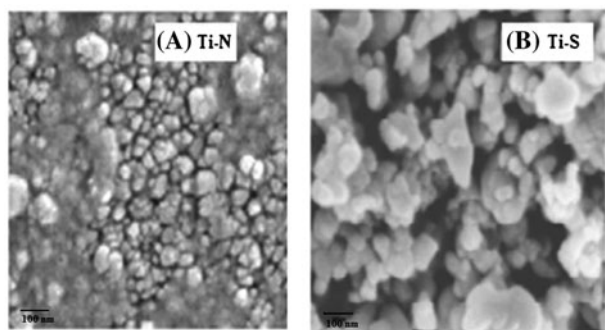| Catalyst	Properties						EDX composition, %			Band gap energy, eV
	Crystallite size, nm	Avg particle size, nm	Specific surface area, m² gm⁻¹	Pore radius, Å	Pore volume, m² gm⁻¹	Anatase, %	Ti	O	NM[a]	
Ti–N	6.23	6.84	208.86	3.05	0.18	100	63.05	33.44	3.51	2.23
Ti–S	12.46	13.13	108.80	0.83	0.10	8.13	67.17	27.88	4.94	3.34

[a]Non-metal N/S.

Fig. 4. SEM images of (A) Ti–N and (B) Ti–B.

The peak located at the binding energy of 167.4 eV and is assigned to the S^{4+} state, while the peak located at the binding energy of 168.5 eV represents the sulfur in the form of S^{6+} [22].

The IR spectra of the non-metal doped catalysts are represented in Fig. 8. In all the figures, a strong broad band near 3,420.0 cm^{-1} could be attributed to the stretching vibration of the hydroxyl group and the interlayer water molecules [23]. This phenomenon was mainly caused by Ti–O–H stretching vibration and the powder surface adsorption. The band near 1,630 cm^{-1} for all samples can be assigned to the bending vibration of H–O–H bond on TiO$_2$ catalyst [24]. This absorption band assigned to the strongly H-bonded H–O–H species is believed to be due to surface-adsorbed water and hydroxyl groups. The band at 420–470 cm^{-1} is attributed to the stretching vibration of Ti–O which is the characteristic IR adsorption band of crystalline TiO$_2$.

For Ti–N catalyst, the strong band at 1,400.82 cm^{-1} was assigned to the characteristic band of NH^{4+}. It was indicated that NH^{4+} adsorbed on the TiO$_2$ surface
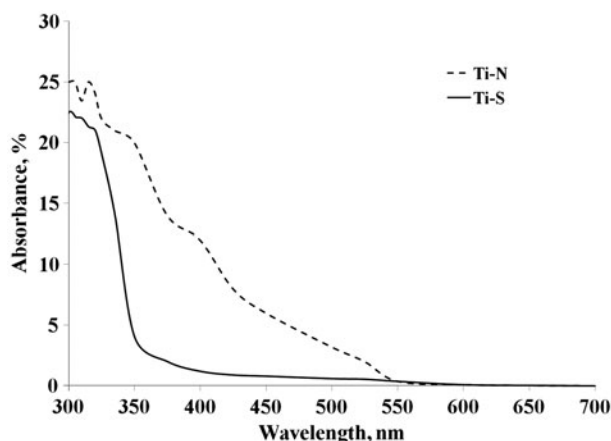

Fig. 6. UV-DRS spectra and band-gap energy of Ti–N and Ti–S.

during the process of preparation, dehydration, and concentration, when heated, N enters the TiO$_2$ crystal lattice and finally forms Ti–N under the high temperature.

From Fig. 8(b) representing the spectra of Ti–S, the peaks located at 1,040, 1,130, and 1,202 cm^{-1} are the characteristic frequencies of sulfate coordinated to metal (such as Ti^{4+}) in bidentate model. The peak at 1,040.12 cm^{-1} is assigned to the S–O stretching frequencies in S–O-Ti, and the peaks at 1,130.12 and 1,202 cm^{-1} belong to S–O stretching frequencies of bridged bidentate sulfate.

3.2. Comparison on PCD% of the non-metal doped catalyst

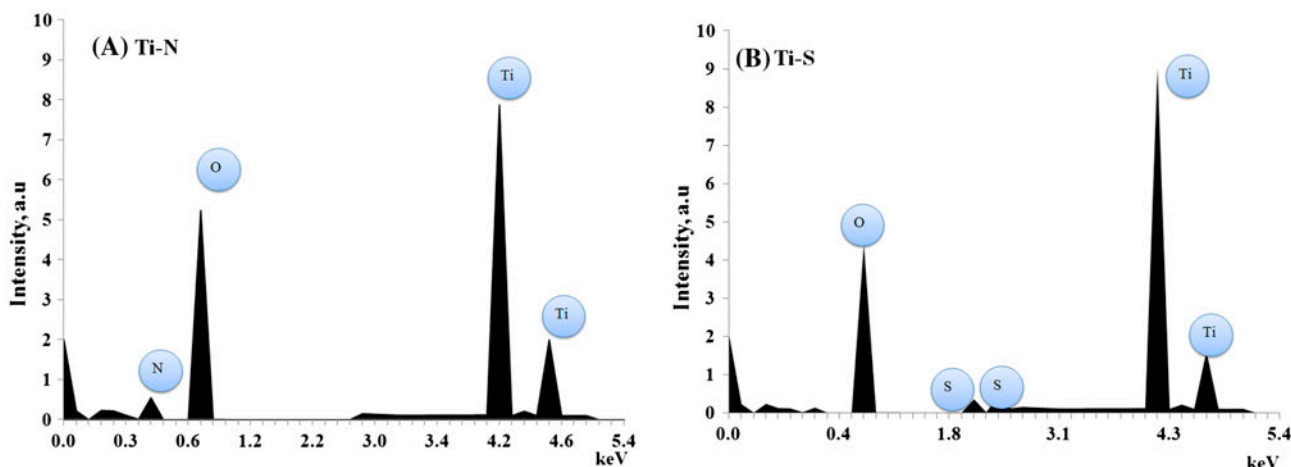The photocatalytic activity and TOC removal of the non-metal-doped catalyst were compared in Fig. 9.

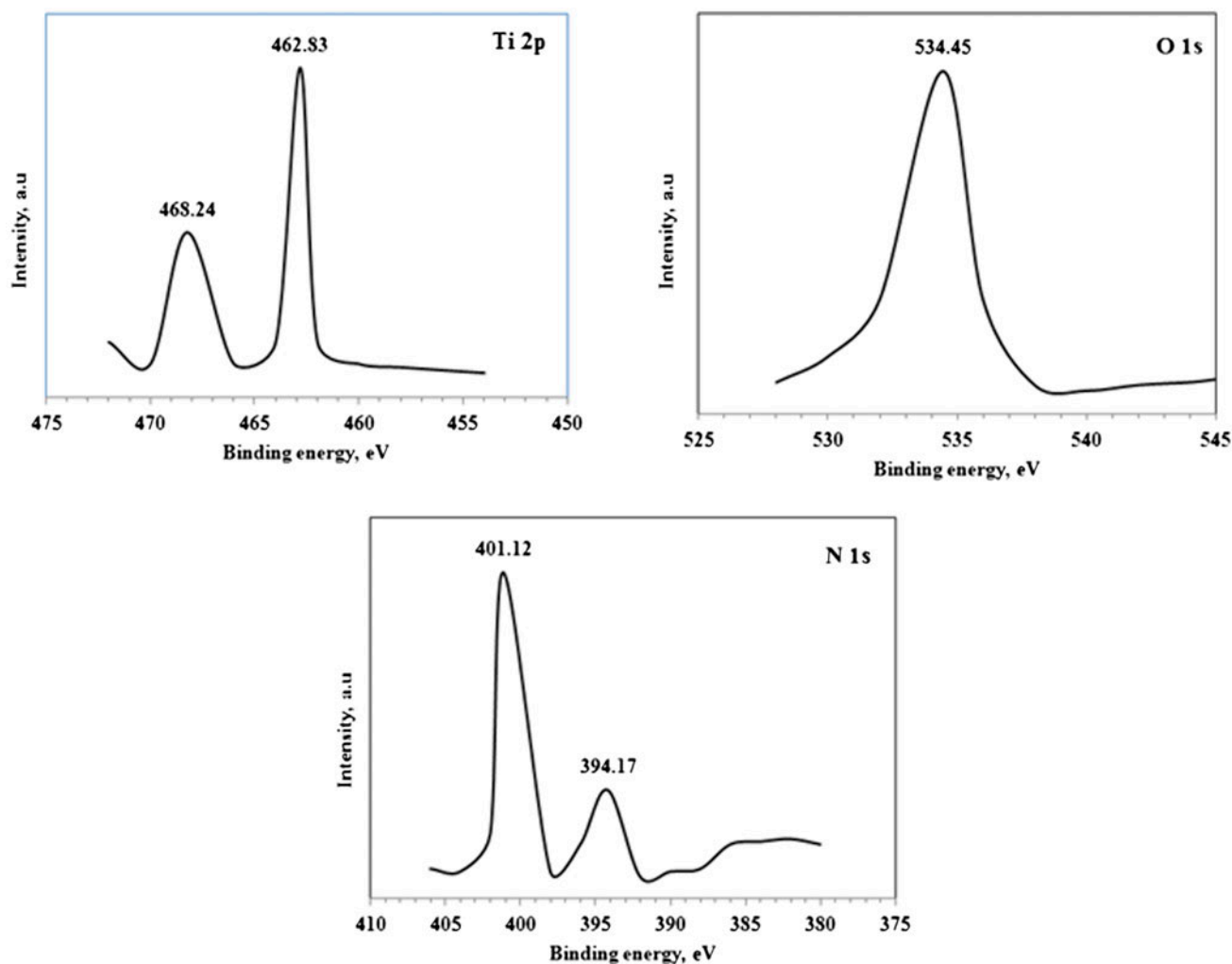Fig. 5. EDX analysis of (A) Ti–N and (B) Ti–S.

Fig. 7(a). XPS spectra of Ti–N catalyst.

3,4-DCA was degraded 100% using Ti–N catalyst in 120 min. The observed PCD % was increased greatly compared to the undoped TiO₂ (sol). Using Ti–S catalyst under the same experimental conditions showed activity less than Ti–N.

It has been observed that the mineralization of the compound proceeds much more rapidly in the presence of N-doped catalyst in visible light. The reason for better photoactivity could be attributed to the fact that the catalyst is composed of nano-crystalline anatase form. The band-gap energy is lower than that of pure titania, it shows a stronger absorption in visible light region and the presence of dopant prevents the recombination of photo-generated electrons and holes leading to better photocatalytic activity. Theoretical calculation for substitutional N-doped anatase and rutile TiO₂ was reported by Valentin et al. [25], who found that the photoexcitation mechanism for N-doped anatase was most likely due to the direct excitation of electrons from the N 2p state located within the band gap of the TiO₂ to the conduction band.

3.3. Effect of operational parameters

3.3.1. Effect of solution concentration

The effect of the substrate initial concentration on the degradation of 3,4-DCA was studied at different concentrations varying from 5 to 30 mgL⁻¹ since the pollutant concentration is a very important parameter in water treatment. Experimental results are presented in Fig. 10, which shows that the degradation % depends on the initial concentration of 3,4-DCA. 5 mgL⁻¹ of the 3,4-DCA solution was degraded completely in 110 min with the catalyst dosage of 0.1 gL⁻¹. Maintaining the same experimental conditions, 10 mg L⁻¹ of the solution
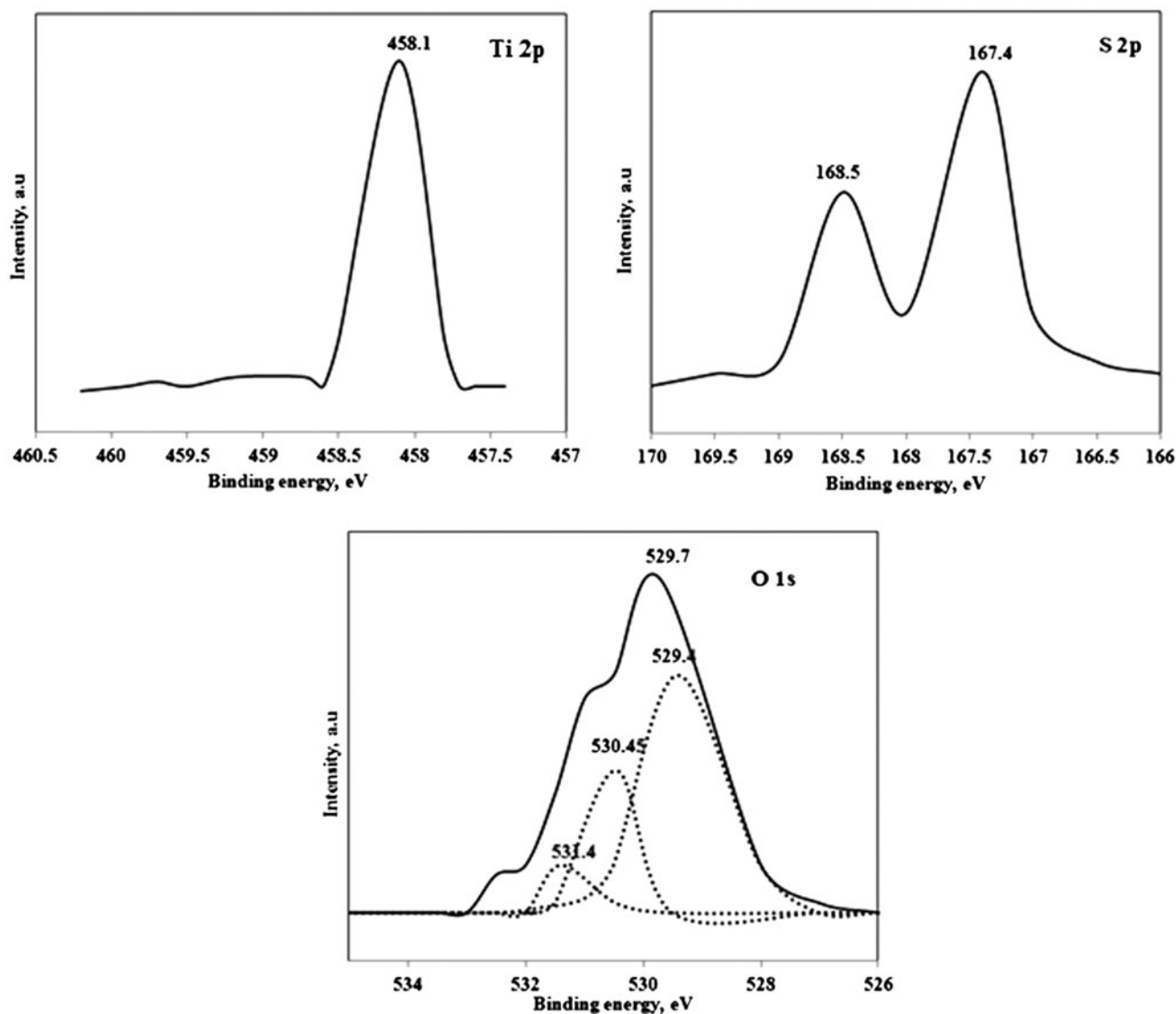
Fig. 7(b). XPS spectra of Ti–S catalyst.

was completely degraded in 120 min. As the concentration was increased, for 15, 20, 25, and 30 mg L^{-1} of 3,4-DCA solution, PCD % achieved was 93, 89, 83, and 79%, respectively.

This may be explained on the basis that upon increasing the concentration of 3,4-DCA, the PCD % decreases as more molecules of the 3,4-DCA are available for degradation. Also with an increase in 3,4-DCA concentration, the solution becomes more intensely colored and the path length of photons entering the solution is decreased; thereby, fewer photons reached the catalyst surface. Hence, the production of hydroxyl and superoxide radicals is reduced [26]. Therefore, the photodegradation efficiency is reduced. Moreover, at the higher concentration, the number of collisions between 3,4-DCA increases whereas the number of collisions between 3,4-DCA molecules and ·OHOH radical decreases. Consequently, the degradation % is retarded [27].

3.3.2. Effect of pH

The effects of pH on the photocatalytic degradation of 3,4-DCA are shown in Fig. 11(a). According to the degradation processes carried out in pH 2–12, the most efficient degradation is in the case of pH 6 and the least one is in the case of pH 12. 100% degradation was achieved at pH 6 in 110 min.
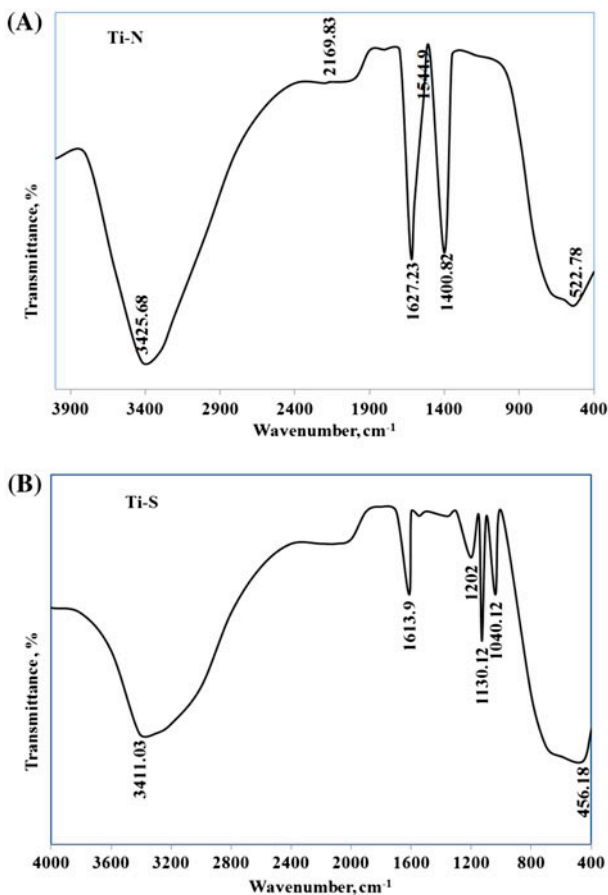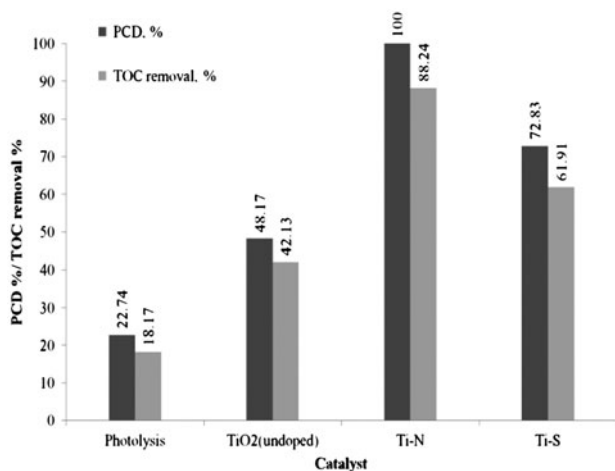
Fig. 8. IR spectra of (A) Ti–N and (B) Ti–S.

Fig. 10. Effect of solution concentration on PCD % (DCA conc.: 5–30 mg L^{-1}, catalyst dosage: 0.1g L^{-1}, visible light intensity: 500 W, visible light irradiation: 120 min, temp: 30°C, and pH 6.8).

The zeta potential before and after doping measured using zeta-meter is represented in Fig. 11(b) as a function of the pH. The zeta potential (Z_{pc}) measured for TiO_2(undoped) showed a value of 6.5 and for Ti–N showed a value of 7. The degradation was achieved the maximum at the pH 6 which almost well supported by the Z_{pc} value also. Because the surface of TiO_2 catalysts in aqueous solution is in the form of Ti–OH, in circumstance of pH value less than the 7, the major species on the surface of catalysts in the form of Ti^- is likely to occur whereas with a pH greater than 7, the negative form of $Ti–O^-$ is prone to happen. To produce strong performance of the photocatalytic reaction, it is important to have fair interaction between the substance to be degraded and the catalysts [28]. Therefore, the pH value of the solution plays a significant role in the interactions between the surface of TiO_2 and the instinctive electron property of the degrading substance.

3.3.3. Effect of light intensity

Experiments were conducted at different light intensities (150, 300, and 500 W) with initial 3,4-DCA concentration of 10 mg L^{-1} and Ti–N loading of 0.1 g L^{-1}, and PCD % was measured at known intervals of time. The PCD % of 3,4-DCA was plotted as shown in Fig. 12. At light intensity of 150 W, 30 min after irradiation, the degradation of 3,4-DCA was found to be 38% and then, removal efficiency increased with time and reached about 88.09% at 120 min. At light

Fig. 9. Comparison of photocatalytic degradation % and TOC removal % using different type of catalyst on degradation of 3,4-DCA (DCA conc.: 10 mg L^{-1}, catalyst dosage: 0.1 g L^{-1}, visible light intensity: 500 W, visible light irradiation: 120 min, photolysis: 420 min, and temp: 30°C).
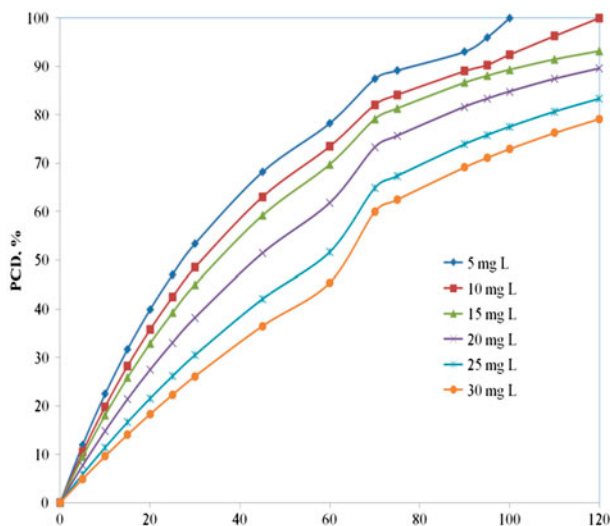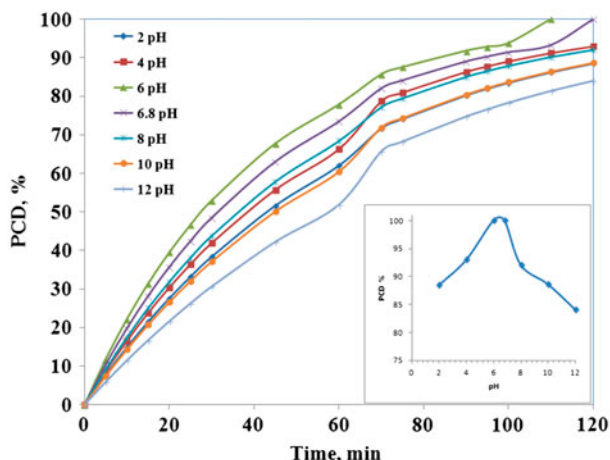
Fig. 11(a). Effect of solution pH on PCD % (DCA conc.: 5–30 mg L^{-1}, catalyst dosage: 0.1g L^{-1}, visible light intensity: 500 W, visible light irradiation: 120 min, temp: 30℃, and pH 2–12).
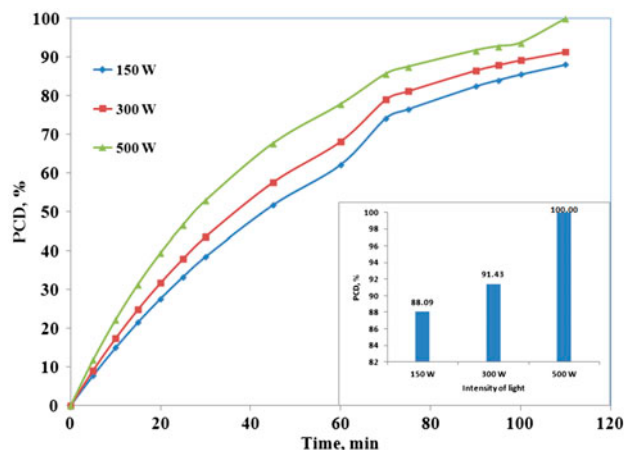

Fig. 12. Effect of light intensity on PCD % (DCA conc.: 10 mg L^{-1}, catalyst dosage: 0.1 g L^{-1}, visible light intensity: 150, 300, 500 W, visible light irradiation: 110 min, temp: 30℃, and pH 6).

that light intensity is one of the important factors influencing photocatalytic degradation of 3,4-DCA.

3.3.4. Effect of catalyst dosage

To ensure the total absorption of photons generated during irradiation of the catalyst and to avoid use of excess catalyst, the optimization of the catalyst dosage is important. Experiments were performed by varying the amount of catalysts from 0.025 to 0.15 g L^{-1}. The solution concentration taken for this optimization study was 10 mg L^{-1} and irradiated using 500 W visible light. The solution pH was adjusted to 6 as it was the optimized pH. The PCD % was determined for different times and plotted in Fig. 13. The percentage of removal increases with increase in dose of the catalysts from 86.37% to 100% for catalyst dosage of 0.025 to 0.1 g L^{-1}. On further increase, the PCD % decreased to 90.20%. Hence, the optimum dosage was found to be 0.1 g L^{-1}.

The increase in PCD % was due to the increase in the number of surface active sites and enhanced generation of hydroxyl radicals due to increase in the concentration of charge carriers. However, at higher catalyst loading, that is, beyond 0.1 g L^{-1}, the reaction rate decreased due to the deactivation of activated molecules by collision with ground state molecules, the agglomeration of the catalyst particles and turbidity at higher catalyst loading results in the shadowing and increase in opacity. Hence, above a certain level, the additional catalyst amount does not get involved in catalytic activity and further increment in the PCD % was not observed [30,31]. Hence, the optimum level of dose is 0.1 g L^{-1}.
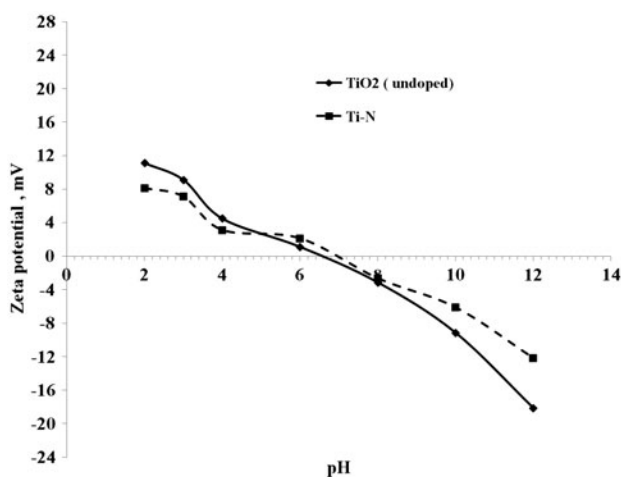

Fig. 11(b). Zeta potential of analysis of undoped TiO$_2$ and Ti–N as function of pH.

intensity of 300 W, the PCD % slowly increased with time and reached about 91.43% at 120 min. At light intensity of 500 W, the PCD % slowly increased with time and reached about 100% at 120 min.

The highest 3,4-DCA removal efficiency was found at the highest light intensity used in this study (500 W). Electron–hole pair generation rate increases with increase in light intensity. Higher intensity of the incident light, which has sufficient-energy, would lead to higher electron–hole pair generation rate, and subsequently higher photocatalytic activity, resulting in higher removal efficiency [29]. This finding indicates
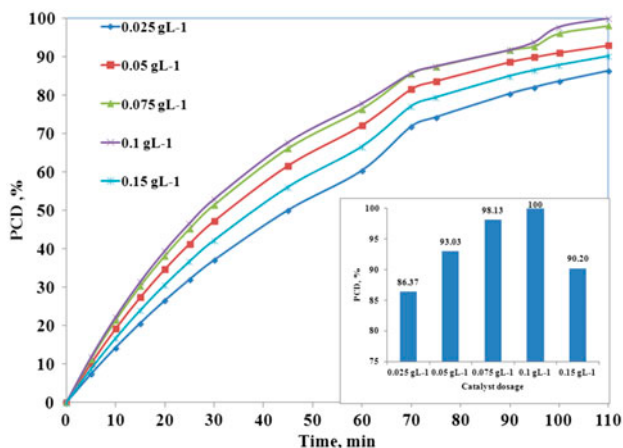
Fig. 13. Effect of catalyst dosage on PCD % (DCA conc.: 10 mg L^{-1}, catalyst dosage: 0.025–0.15g L^{-1}, visible light intensity: 500 W, visible light irradiation: 110 min, temp: 30℃, and pH 6).

3.4. Langmuir–Hinshelwood Kinetics

The kinetics of the degradation reaction is conventionally described by the Langmuir–Hinshelwood kinetics (L–H) [32], which takes into account the adsorption of the compound over the surface of the catalyst, surface reaction, and desorption of the products. The rate of reaction following L–H kinetics can be given as Eq. (5).

$$r = \frac{k_r K_{LH} C}{1 + K_{LH} C} \tag{5}$$

where r is the rate of degradation of compound, k_r is the rate constant for the degradation of the compound,

K_{LH} is the adsorption equilibrium constant, and C is the concentration of the compound in the solution.

As a simplified L-H rate equation (Eq. (5)) renders a simple pseudo-first-order kinetic equation, k values could be deduced from a slope of ln (C_0/C) vs. irradiation time plot, as shown in Fig. 14. From the deduced k values, the values of k_r and K_{LH} were calculated by the plot of $1/k$ vs C_0 as shown in Fig. 15 and the half-life values at different solution concentration as shown in Fig. 16. The rate constants were determined for two regimes, that is, for 0–60 min and 60–120 min since there were two kinetic regime formed and single straight fit for the entire time period did not fit well as seen from the regression coefficient being low. In the two-regime fit, the rate constant determined for the initial time (0–60 min) was lower than for the latter regime (60–120 min). Similar behavior was seen, when 3,4-DCA was degraded using Ti–V catalyst [2].

The reaction rate constant k_{r1} and k_{r2} was calculated and was found to decrease with solution concentration and increase with intensity of light. There was no difference between K_{LH1} and K_{LH2} values as seen from Table 3. The values of reaction rate constant were much higher than K_{LH} which indicates that the photoreaction dominates the degradation, but not adsorption.

Half-life time $t_{1/2}$ was calculated using the following Eq. (6) and (7). While Eq. (6) deduced from Eq. (5) which yields $t_{1/2}$ experimental values, Eq. (7) is the $t_{1/2}$ for first-order reaction, that is, $t_{1/2}$ (theoretical).

$$t_{1/2(\text{experimental})} = \left(\frac{0.693}{k_r K_{LH}}\right) + \left(\frac{0.5 \times C_0}{k_r}\right) \tag{6}$$
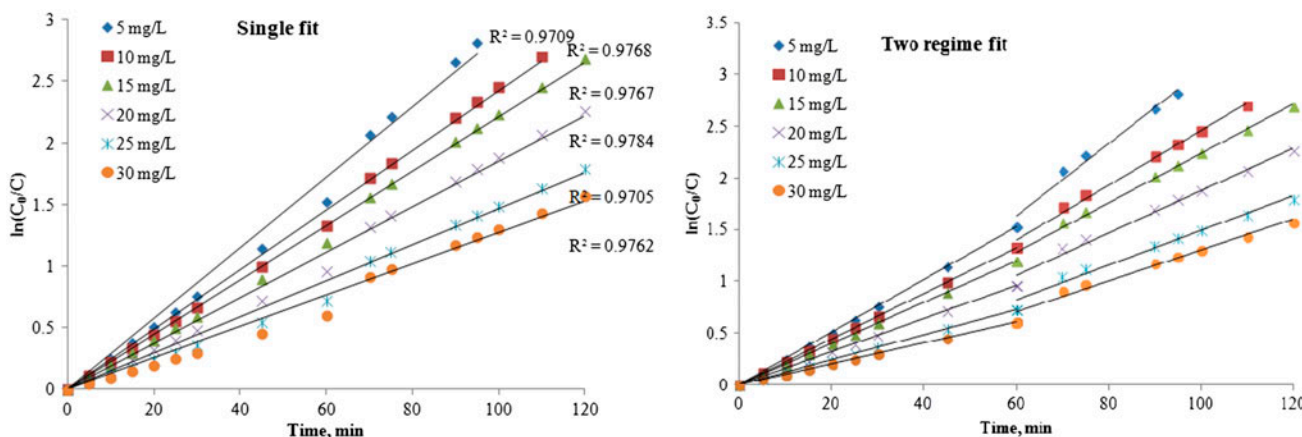

Fig. 14. LH kinetic model fit for different concentration (DCA conc.: 5–30 mg L^{-1}, catalyst dosage: 0.1 g L^{-1}, visible light intensity: 500 W, visible light irradiation: 120 min, temp: 30℃, and pH 6.8).
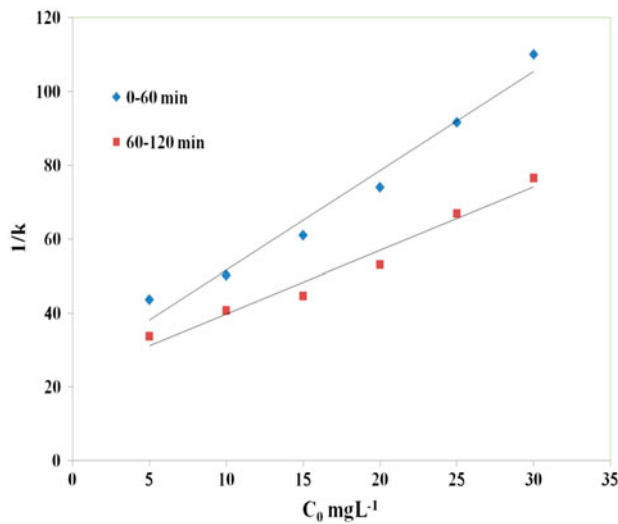
Fig. 15. Determination of reaction constant and adsorption constant for different concentration (DCA conc.: 5–30 mg L^{-1}, catalyst dosage: 0.1 g L^{-1}, visible light intensity: 500 W, visible light irradiation: 120 min, temp: 30℃, and pH 6.8).

Fig. 17. Comparison of electric energy per order for different types of catalyst.

the two-regime fit was found to be almost similar, instead $t_{1/2}$ calculated for the experimental and theoretical values using the reaction rate constant and adsorption constant from the single fit showed a vast deviation. Hence, the two-regime fit was found to be more appropriate L–H kinetic fit than single fit.

3.5. Power consumption

The evaluation of the treatment costs is, at the moment, one of the aspects that need more attention. Economics, economy of scale, regulations, effluent quality goals, operation, maintenance and control and robustness are the important factors for selecting any wastewater treatment technology. The visible light irradiated Ti–N catalyst is an electric energy intensive process. Electric energy represents a major fraction of the operating costs. In the case of low pollutant concentration, the appropriate figure-of-merit is the EEO and defined as the number of kilowatt hours of electrical energy required to reduce the concentration of a pollutant by 1 order of magnitude in a unit volume of contaminated water [33]. The EEO (kWh/m^3/order) can be calculated from the following Eq. (8) for a batch type reactor:
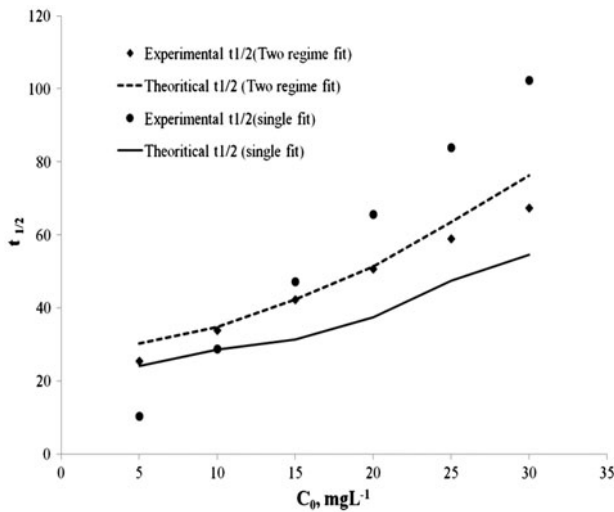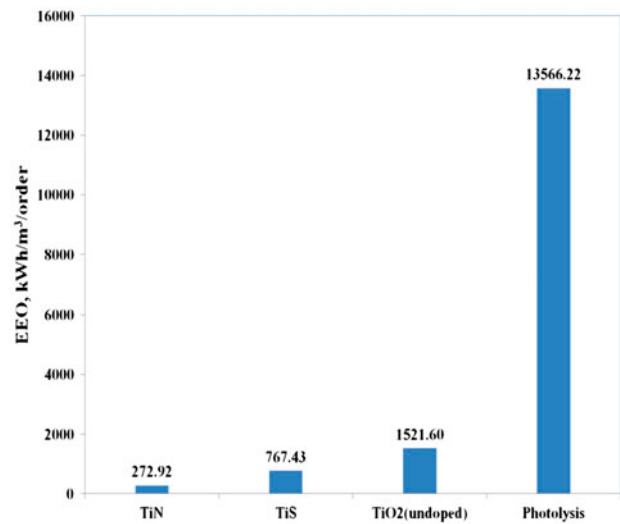

Fig. 16. Comparison of the experimental and theoretical half-life time of 3,4-DCA for different concentration (DCA conc.: 5–30 mg L^{-1}, catalyst dosage: 0.1 g L^{-1}, visible light intensity: 500 W, visible light irradiation: 120 min, temp: 30℃, and pH 6.8).

$$t_{1/2(\text{theoritical})} = \left(\frac{0.693}{k} \right) \tag{7}$$

From the plot as shown in Fig. 16, the $t_{1/2}$ calculated from the experimental and theoretical values using the reaction rate constant and adsorption constant from

Electrical energy per order (EEO) kWhm^{-3}/order

$$= \frac{P \times t \times 1{,}000}{V \times 60 \times \ln\left(\frac{C_0}{C}\right)} \tag{8}$$

where P is the input power (kW) to the AOP system, t is the irradiation time (min), V is the volume of water

Table 3
Kinetic parameter for degradation of 3,4-DCA

C_0, mg L^{-1}	Rate constant		Reaction constant, min^{-1}		Adsorption constant, L mg^{-1}		Half life time, ($t_{1/2}$) min	
	k_1	k_2	k_{r1}	k_{r2}	K_{LH1}	K_{LH2}	theo.	exp.
5	0.0255	0.0296	1.169	2.182	0.061	0.062	25.47	27.23
10	0.0221	0.0245					33.84	31.33
15	0.0199	0.0224					42.22	34.77
20	0.0160	0.0188					50.60	43.20
25	0.0121	0.0149					58.98	57.18
30	0.0101	0.0131					67.36	68.68

(l) in the reactor, and C_0 and C are the initial and final pollutant concentrations, respectively (Fig. 17).

The EEO values for degradation of 3,4-DCA by photolysis, TiO$_2$ (undoped), Ti–N, and Ti–S using 500 W visible light were 13,566.22, 1,521.60, 767.43, and 272.92 kWh/m^3/order, respectively. The EEO values showed that electrical efficiency in the photocatalysis process is better than in photolysis system. It is also clear that the photocatalytic process in presence of Ti–N offered the best energy efficiency.

4. Conclusions

In this study, Ti–N and Ti–S were prepared using sol–gel method and characterized. Ti–N catalyst was found to be better in terms of band-gap shift, particle size, and specific surface area. The PCD % of 3,4-DCA was maximum with Ti–N using 500 W visible light. The operational parameters were optimized as follows: light intensity: 500 W, catalyst dosage: 0.1 g L^{-1}, concentration: 5–10 mg L^{-1}, and pH 6. The L–H kinetics model was used for determining rate constants and adsorption constants. Kinetics did not follow LH single fit model. The kinetics followed two-regime fit for 0–60 min and 60–120 min. The half-life time was calculated and found to be in close approximation to the theoretical values. The EEO for Ti–N was found to be 272 kWh/m^3/order and the least compared to other type of catalyst.

References

[1] J.V. Pothuluri, J.A. Hinson, C.E. Cerniglia, Propanil: Toxicological characteristics, metabolism, and biodegradation potential in soil, J. Environ. Qual. 20 (1991) 330–347.

[2] E. Padmini, L.R. Miranda, Nanocatalyst from sol–sol doping of TiO$_2$ with Vanadium and Cerium and its application for 3,4-Dichloroaniline degradation using visible light, Chem. Eng. J. 232 (2013) 249–258.

[3] D.K. Lee, S.C. Kim, I.C. Cho, S.J. Kim, S.W. Kim, Photocatalytic oxidation of microcystin-LR in a fluidized bed reactor having TiO$_2$-coated activated carbon, Sep. Purif. Technol. 34 (2004) 59–66.

[4] M.N. Chong, V. Vimonses, S. Lei, B. Jin, C. Chow, C. Saint, Synthesis and characterisation of novel titania impregnated kaolinite nano-photocatalyst, Microporous Mesoporous Mater. 117 (2009) 233–242.

[5] H. Zhu, X. Gao, Y. Lan, D. Song, Y. Xi, J. Zhao, Hydrogen titanate nanofibers covered with anatase nanocrystals: A delicate structure achieved by the wet chemistry reaction of the titanate nanofibers, J. Am. Chem. Soc. 126 (2004) 8380–8381.

[6] S.Y. Kwak, S.H. Kim, Hybrid organic/inorganic reverse osmosis (RO) membrane for bactericidal antifouling. 1. Preparation and characterization of TiO$_2$ nanoparticle self assembled aromatic polyamide thin-film-composite (TFC) membrane, Environ. Sci. Technol. 35 (2001) 2388–2394.

[7] J.A. Byrne, B.R. Eggins, Photoelectrochemistry of oxalate on particulate TiO$_2$ electrodes, J. Electroanal. Chem. 457 (1998) 61–72.

[8] O. Carp, C.L. Huisman, A. Reller, Photoinduced reactivity of titanium dioxide, Prog. Solid State Chem. 32 (2004) 33–177.

[9] Z. Ambrus, K. Mogyorósi, A. Szalai, T. Alapi, K. Demeter, A. Dombi, P. Sipos, Low temperature synthesis, characterization and substrate—Dependent photocatalytic activity of nanocrystalline TiO$_2$ with tailor–made rutile to anatase ratio, Appl. Catal. A 340 (2008) 153–161.

[10] D.B. Hamal, K.J. Klabunde, Synthesis, characterization, and visible light activity of new nanoparticle photocatalysts based on silver, carbon, and sulphur doped TiO$_2$, J. Colloid Interface Sci. 311 (2007) 514–522.

[11] M. Iwasaki, M. Hara, H. Kawada, H. Tada, S. Ito, Cobalt ion-doped TiO$_2$ photocatalyst response to visible light, J. Colloid Interface Sci. 224 (2000) 202–204.

[12] J. Zhu, F. Chen, J. Zhang, H. Chen, M. Anpo, Fe^{3+}-TiO$_2$ photocatalysts prepared by combining sol–gel method with hydrothermal treatment and their characterization, J. Photochem. Photobiol. C 180 (2006) 196–204.

[13] X.Z. Li, F.B. Li, Study of Au/Au^{3+}-TiO$_2$ photocatalysts towards visible photooxidation for water and wastewater treatment, Environ. Sci. Technol. 35 (2001) 2381–2387.

[14] D. Behar, J. Rabani, Kinetics of hydrogen production upon reduction of aqueous TiO$_2$ nanoparticles catalyzed by Pd^0, Pt^0, or Au^0 coatings and an unusual hydrogen abstraction; steady state and pulse radiolysis study, J. Phys. Chem. B 110 (2006) 8750–8755.

[15] Y. Zeng, W. Wu, S. Lee, J. Gao, Photocatalytic performance of plasma sprayed Pt-modified TiO$_2$ coatings under visible light irradiation, Catal. Commun. 8 (2007) 906–912.

[16] N. Ghows, M.H. Entezari, Fast and easy synthesis of core-shell nanocrystal (CdS/TiO$_2$) at low temperature by micro-emulsion under ultrasound, Ultrason Sonochem. 18 (2011) 629–634.

[17] R. Brahimi, Y. Bessekhouad, A. Bouguelia, M. Trari, Visible light induced hydrogen evolution over the heterosystem Bi$_2$S$_3$/TiO$_2$, Catal. Today 122 (2007) 62–65.

[18] J.S. Jang, S.M. Ji, S.W. Bae, H.C. Son, J.S. Lee, Optimization of CdS/TiO$_2$ nano-bulk composite photocatalysts for hydrogen production from Na$_2$S/Na$_2$SO$_3$ aqueous electrolyte solution under visible light (λ ≥ 420 nm), J. Photochem. Photobiol. A 188 (2007) 112–119.

[19] K. Demeestere, J. Dewulf, T. Ohno, P.H. Salgado, H. Van Langenhove, Visible light mediated photocatalytic degradation of gaseous trichloroethylene and dimethyl sulfide on modified titanium dioxide, Appl. Catal. B 61 (2005) 140–149.

[20] R.A. Spurr, H. Myers, Quantitative analysis of anatase–rutile mixtures with an X-Ray diffractometer, Anal. Chem. 29 (1957) 760–762.

[21] T. Horikawa, M. Katoh, T. Tomida, Preparation and characterization of nitrogen-doped mesoporous titania with high specific surface area, Microporous Mesoporous Mater. 110 (2008) 397–404.

[22] T. Ohno, M. Akiyoshi, T. Umebayashi, K. Asai, T. Mitsui, M. Matsumura, Preparation of S-doped TiO$_2$ photocatalysts and their photocatalytic activities under visible light, Appl. Catal. A 265 (2004) 115–121.

[23] J.J. Liu, X.P. Li, S.L. Zuo, Y.C. Yu, Preparation and photocatalytic activity of silver and TiO$_2$ nanoparticles/montmorillonite composites, Appl. Clay Sci. 37 (2007) 275–280.

[24] Y.X. Li, G.F. Ma, S.Q. Peng, G.X. Lu, S.B. Li, Boron and nitrogen co-doped titania with enhanced visible-light photocatalytic activity for hydrogen evolution, Appl. Surf. Sci. 254 (2008) 6831–6836.

[25] C.D. Valentin, G. Pacchioni, A. Selloni, Origin of the different photoactivity of N-doped anatase and rutile TiO$_2$, Phys. Rev. B 70 (2004) 0851161–0851164.

[26] A.K. Subramani, K. Byrappa, S. Ananda, K. Lokanatha Rai, Photocatalytic degradation of indigo carmine dye using TiO$_2$ impregnated activated carbon, Bull. Mater. Sci. 30 (2007) 37–41.

[27] S. Lodha, D. Vaya, R. Ameta, P.B. Punjabi, Photocatalytic degradation of phenol red using complexes of some transition metals and hydrogen peroxide, J. Serb. Chem. Soc. 73 (2008) 631–639.

[28] A. Piscopo, D. Robert, J.V. Weber, Influence of pH and chloride anion on the photocatalytic degradation of organic compounds Part I. Effect on the benzamide and para-hydroxybenzoic acid in TiO$_2$ aqueous solution, Appl. Catal. B 35 (2001) 117–124.

[29] D.F. Ollis, E. Pelizzetti, N. Serpone, Photocatalyzed destruction of water contaminants, Environ. Sci. Technol. 25 (1991) 1522–1529.

[30] S. Anandan, T. Narasinga Rao, M. Sathish, D. Rangappa, I. Honma, M. Miyauchi, Superhydrophilic graphene-loaded TiO$_2$ thin film for self-cleaning applications, ACS Appl. Mater. Interfaces 5 (2013) 207–212.

[31] A. Ye, W. Fan, Q. Zhang, W. Deng, Y. Wang, CdS–graphene and CdS–CNT nanocomposites as visible-light photocatalysts for hydrogen evolution and organic dye degradation, Catal. Sci. Technol. 2 (2012) 969–978.

[32] A. Mills, S. Morris, Photo-mineralization of 4-chlorophenol sensitized by titanium dioxide: A study of the initial kinetics of carbon dioxide photo-generation, J. Photochem. Photobiol. A 71 (1993) 75–83.

[33] J.R. Bolton, K.G. Bircher, K.G.W. Tumas, C.A. Tolman, Figures-of-merit for the technical development and application of advanced oxidation technologies for both electric- and solar-driven systems, Pure Appl. Chem. 73 (2001) 627–637.